TU Delft

Delft University of Technology

# Joint Doppler and DOA estimation using (Ultra-)Wideband FMCW signals

Xu, Shengzhi; Kooij, Bert Jan; Yarovoy, Alexander

**DOI**
10.1016/j.sigpro.2019.107259

**Publication date**
2020

**Document Version**
Final published version

**Published in**
Signal Processing

**Citation (APA)**
Xu, S., Kooij, B. J., & Yarovoy, A. (2020). Joint Doppler and DOA estimation using (Ultra-)Wideband FMCW signals. *Signal Processing*, *168*, Article 107259. https://doi.org/10.1016/j.sigpro.2019.107259

**Important note**
To cite this publication, please use the final published version (if applicable).
Please check the document version above.

**Copyright**
Other than for strictly personal use, it is not permitted to download, forward or distribute the text or part of it, without the consent of the author(s) and/or copyright holder(s), unless the work is under an open content license such as Creative Commons.

**Takedown policy**
Please contact us and provide details if you believe this document breaches copyrights.
We will remove access to the work immediately and investigate your claim.

*This work is downloaded from Delft University of Technology.*
*For technical reasons the number of authors shown on this cover page is limited to a maximum of 10.*

***Green Open Access added to TU Delft Institutional Repository***

***'You share, we take care!' – Taverne project***

***https://www.openaccess.nl/en/you-share-we-take-care***

Otherwise as indicated in the copyright section: the publisher is the copyright holder of this work and the author uses the Dutch legislation to make this work public.

Signal Processing 168 (2020) 107259

Contents lists available at ScienceDirect

Signal Processing

journal homepage: www.elsevier.com/locate/sigpro

# Joint Doppler and DOA estimation using (Ultra-)Wideband FMCW signals

Shengzhi Xu*, Bert Jan Kooij, Alexander Yarovoy

*Delft University of Technology, Delft 2628 CD, the Netherlands*

ARTICLE INFO

*Article history:*
Received 28 January 2019
Revised 26 May 2019
Accepted 15 August 2019
Available online 4 September 2019

*Keywords:*
Ultra-Wideband (UWB)
Direction-of-Arrival (DOA)
Doppler
2 Dimensional multiple signal classification (2D MUSIC)
Lanczos algorithm
Rayleigh–Ritz step

ABSTRACT

The joint Doppler and Direction-of-Arrival (DOA) estimation of moving targets using an (Ultra-)Wideband (UWB) frequency modulated continuous-wave (FMCW) antenna array radar is investigated. Besides the well-known range migration problem, another concern for wideband signals is the DOA estimation problem. For the first time, both problems are considered in this paper simultaneously, where the wideband DOA is transformed into a second-order coupling system similar to the range migration problem by using the property of the FMCW signal. A novel embedded compensation approach to eliminate the coupling terms caused by range migration and wideband DOA is proposed and 2D multiple signal classification (2D MUSIC) algorithm is subsequently applied with dynamic noise subspace to joint estimation of Doppler and DOA. Further, to reduce the computational load caused by multiple eigendecompositions of large matrices, efficient implementation methods are proposed and their performance in speed, accuracy and robustness is compared. The performance of the proposed methods is validated by the numerical simulations and is compared with Keystone MUSIC. Finally, it is shown that for a small number of targets, the Rayleigh-Ritz is the most efficient approach among them.

© 2019 Elsevier B.V. All rights reserved.

## 1. Introduction

Detection and localization of moving targets are important in many fields such as automotive radar [1], ground moving target indication (GMTI) [2], underwater acoustic array [3]. The most important parameters of moving targets are the range, azimuthal (and, in 3D space, elevation) angle (or DOA) and velocity. The target range and angle together determine the location of a target. While the Doppler (along with range) velocity is determined in coherent radars by means of phase shift between chirps within the coherent processing interval (CPI), and DOA is determined from the phase shift of signals received by different antennas within antenna array. Both phase shifts can be easily measured separately using narrowband radar. Using the de-chirping technique for FMCW radar [2,4], the received signals are transformed into multi-dimensional complex sinusoids (whose phase depends on the fast-time - range, slow-time - Doppler velocity and array element - DOA). Then the estimation of targets parameters is transformed into the frequencies estimation problem. By extending traditional single-frequency estimators to joint multiple frequencies estimators, such as matched filter, 2D-Capon [5], 2D-MUSIC [6], 2D-ESPRIT [7] and sparse representation methods [8,9], joint range-Doppler estimation algorithms have been developed. These algorithms perform well under narrow-band signal condition. Target movement causes, however, change in the target range during one CPI (physically) and the cross-couplings between fast-time and slow-time (mathematically), which is called range migration or range walk in GMTI [2,10,11]. The cross-coupling terms spread the Fourier spectrum and consequently lead to estimation errors for these classic algorithms: the larger the signal bandwidth or the higher the target velocity, the higher the estimation error of conventional methods [10,12].

Recently, since wideband signals are widely used due to the demand of increasingly higher range resolution, the range migration problem has attracted significant attention. To solve the target migration problem, the relaxation-based super-resolution algorithms have been proposed in [2,13,14] for multiple moving target feature extractions. However, they consider a wide-band approach for the range profile, while they assume a narrow-band approach for the steering vector. In [15], the authors present the iterative adaptive algorithm (IAA) for joint multiple parameters estimation, which provides super-resolution by iteratively calculating the covariance matrix together with estimation results. In [16,17], IAA is extended to the wideband waveform case together with the range migration problem. However, IAA consumes a huge amount of memory and time when the raw data dimension is large and

* Corresponding author.
*E-mail address:* s.xu-4@tudelft.nl (S. Xu).

https://doi.org/10.1016/j.sigpro.2019.107259
0165-1684/© 2019 Elsevier B.V. All rights reserved.

the scanning area is divided into dense bins, which makes the algorithm impractical for real-time applications. The Keystone transform and matched filter are used in [12,18] to eliminate the range walk residual and the Radon Fourier transform (RFT) is proposed to consider even higher-order coupling problems by line or curve searching in the time domain in [10,19]. Unfortunately, these approaches need a large amount of raw data to do interpolation or coherent integration, therefore. They could not provide the same fine resolution as the super-resolution algorithms in [6,15]. Implementation of the RFT also requires a large amount of computing power for the line searching in multi-dimensional data. Some waveform design methods are also proposed to solve the range migration problem [11], but these algorithms increase the system's complexity and the achieved resolution is not as high as that obtained by super-resolution algorithms.

In addition to the range migration, another limitation for (Ultra-)WB signal in the collocated array or multiple-input and multiple-output (MIMO) application is the DOA estimation. Although the range migration problem has been studied intensively, the current algorithms jointly dealing with range migration and DOA estimation fail to provide a good solution to wideband DOA estimation by simplifying the signal model with narrowband DOA assumption [2,14,20]. The traditional DOA estimators are based on narrowband assumptions by the interferometry information, such as Capon, MUSIC, etc. To apply the traditional narrowband super-resolution algorithm for wideband cases, two of the mainstreams of wideband DOA estimation are proposed, namely the incoherent signal subspace method (ISSM) and the coherent signal subspace method (CSSM). ISSM solves this problem via a filter bank to decompose the array output into its independent narrowband components. Then the subspace-based algorithm is applied to each narrowband output, and DOA estimates can be average in some way. However, each of narrowband estimates does not fully exploit the total emitter power and some of the narrowband components may have a low signal-to-noise ratio (SNR), and the final DOA estimates may be adversely affected by few inaccurate narrowband estimates. CSSM combines the different narrowband signal subspace into a single signal subspace that obeys the narrowband array model. Although it is shown in [21] that the performance of CSSM is superior to ISSM, the forming of focusing matrices and universal spatial covariance matrix (USCM) can increase the computational complexity significantly. In addition, the accuracy of the focussing matrices highly depends on and is sensitive to the preliminary estimate of the true DOAs [22]. In some other communication problems, joint time-of-arrival (TOA) and DOA estimation in impulse radio (IR)-UWB is studied, unfortunately, the DOAs are estimated by the pulse delay which is decided by the bandwidth and not suitable for the compact array. Another powerful tool for DOA estimation is the time-frequency(TF)-MUSIC [23,24] which is used to deal with non-stationary sources and it is also applied for wideband DOA estimation in a similar way as CSSM [25]. However, in FMCW radar de-chirped signals (beat frequency signals) for each antenna element and a single FMCW chirp behave as "stationary sources", so an application of TF-MUSIC to them is not helpful.

Although both range migration and wideband DOA estimation are intensively studied separately, there are few articles address both problems simultaneously. In this paper, a MUSIC-based algorithm is proposed for the problem of joint Doppler and DOA estimation using an (ultra)wide-band array-based radar considering both range migration and wideband DOA issues. The range migration model has been studied comprehensively and presented as the second-order coupling between fast-time and slow-time. Combine the fact that the steering vector is the function of the frequency of wideband DOA and the frequency is the function of fast-time in FMCW signal, the conventional CSSM and ISSM can be avoided by transforming the steering vector into the function of fast-time. Thus, the wideband DOA problem is transformed into the inter-coupling between the fast-time and the element indices analogue to the range migration problem. By this transform, both range migration and wideband DOA problem present as coupling terms and can be eliminated in the same way. After establishing the signal model, the classic 2D MUSIC-based algorithm for joint estimation of Doppler and DOA is presented. Unfortunately, conventional 2D MUSIC algorithm cannot correctly estimate the parameters in the presence of the couplings. To eliminate the influence of the coupling terms for accurate parameters estimation, a phase compensation method is proposed for both couplings of range migration and wideband DOA. The compensation method needs, however, multiple large-size matrix eigendecompositions which are computationally heavy. Therefore, two efficient implementations, namely the Lanczos algorithm and Rayleigh–Ritz step, are introduced. We compare the two proposed methods with the inverse method, which is also a general MUSIC accelerating approach presented in [26]. The advantages of the proposed techniques are shown via numerical simulations.

The rest of the paper is organised as follows. In Section 2, we establish the signal model of multiple moving targets for (Ultra-)WB FMCW antenna array radar. In Section 3, the classic 2D MUSIC is applied to joint estimation of Doppler and DOA. Then, the compensation algorithm is proposed. The efficient implementations are introduced and compared in Section 4. Simulation results are presented in Section 5.

Notations used in this paper are as follows. Scalars are denoted by lower-case letters, vectors and matrices are written as lower-case and uppercase bold-face letters, respectively. $(\cdot)^T$, $(\cdot)^H$ and $(\cdot)^*$ denote transpose, conjugate transpose and complex conjugate of a vector or matrix, respectively. $\otimes$ and $\odot$ represent the Kronecker and Hadamard product, respectively. $\lfloor x \rfloor$ gives the nearest integer less than or equal to $x$. $\mathbf{I}_M$ denotes the $M \times M$ identity matrix. Some other special matrices are $\mathbf{1}_M = [1, 1, \ldots, 1]^T \in \mathbb{R}^{M\times 1}$, $\mathbf{d}_M = [0, 1, \ldots, M-1]^T \in \mathbb{R}^{M\times 1}$. Further, the symbols $\mathbb{E}()$, $\mathrm{Tr}()$, $\Re()$ and $\mathcal{O}()$ represent the expectation computation, the trace of a matrix, the real part extraction operation and asymptotic notation, respectively.

## 2. UWB FMCW antenna array model

### 2.1. Array signal model

In this section, the signal model using the mono-static antenna array with one transmitter and $L$ receivers is established. Assume $I$ point targets with unknown range $\mathbf{r} = [R_1, R_2, \ldots, R_I]$, radial velocity $\mathbf{v} = [v_1, v_2, \ldots, v_I]$ and angle $\boldsymbol{\theta} = [\theta_1, \theta_2, \ldots, \theta_I]$ are located in the observed far-field, where $\mathbf{v}$ and $\boldsymbol{\theta}$ are expected to be jointly estimated. The radar transmits a group of chirps during one CPI with the chirp duration $T_0$ and the pulse repetition interval (PRI) $T$. A normalized single chirp signal with the bandwidth $B$ has the form

$$s_0(t) = \begin{cases} e^{j2\pi(f_0 t + 0.5\mu t^2)} & t \in [0, T_0), \\ 0 & t \in (-\infty, 0] \wedge t \in [T_0, \infty), \end{cases} \tag{1}$$

where $f_0$ denotes the starting frequency and $\mu = \frac{B}{T_0}$ denotes the frequency modulation rate. The periodic transmitted signal is decomposed into fast-time domain $t'$ and chirp number domain $m = \lfloor \frac{t}{T} \rfloor$ as (2), where $m = 0, 1, \ldots, M-1$, and $M$ is the total number of chirps in one CPI.

$$t = t' + mT \qquad t' \in [0, T_0). \tag{2}$$

Then the periodic transmitted signal has

$$s(t) = s(t' + mT) = s(m, t') = s_0(t'). \tag{3}$$

Consider the $i$th scatterer in the observation domain with the velocity $v_i$ and the range $R_i$, the round trip time delay of this scatterer is

$$\tau_i(m,t') = \frac{2(R_i + v_i(t'+mT))}{c} = \gamma_i + \frac{2v_i}{c}(t'+mT), \tag{4}$$

where $\gamma_i = \frac{2R_i}{c}$ is the initial round trip delay of the $i$th target for the first chirp and $c$ is the speed of light. Using the 0th element as a reference, the received signal of $i$th scatterer by the $l$th element can be written as

$$\begin{aligned} r_i^{(l)}(m,t') &= \alpha_i \exp(j\varphi_i^{(l)}) s(t'+mT-\tau_i(m,t')) \\ &= \alpha_i \exp(j\varphi_i^{(l)}) s_0(t'-\tau_i(m,t')) \\ &= \alpha_i \exp(j\varphi_i^{(l)}) \exp[j2\pi\phi_i(m,t')], \\ \text{with } t' &\in [\tau_i(m,t_0), T_0), \end{aligned} \tag{5}$$

where $t_0 = \tau_i(m,t_0) = \tau_i(m,0)/(1-2v_i/c)$ is the round trip delay and usually $t_0 << T_0$, the superscript $(l)$ denotes the $l$th element, $l = 0, 1, \ldots, L-1$ denotes the indices of the element and $L$ is the total number of the elements, $\alpha_i$ is the constant complex amplitude of the $i$th scatterer, $\exp(j\varphi_i^{(l)})$ denotes the phase delay relative to the 0th element, and $2\pi\phi_i(m, t')$ is the phase of the received signal of the 0th element, which according to (1) has the form

$$\begin{aligned} \phi_i(m,t') &= f_c(t'-\tau_i(m,t')) + 0.5\mu(t'-\tau_i(m,t'))^2, \\ \text{with } t' &\in [\tau_i(m,t_0), T_0). \end{aligned} \tag{6}$$

From the phase of the received signal, the instantaneous frequency of the received signal is extracted as

$$\begin{aligned} f_i(m,t') &= \frac{d\phi_i(m,t')}{dt'} \\ &= f_c\left(1 - \frac{d\tau_i(m,t')}{dt'}\right) + \mu(t'-\tau_i(m,t'))\left(1 - \frac{d\tau_i(m,t')}{dt'}\right) \\ &\approx f_c + \mu t'. \end{aligned} \tag{7}$$

Now the terms of the time delay are neglected since $\tau_i(m, t') << T_0$ and $v_i << c$. Then the phase delay of the $l$th element is given by

$$\varphi_i^{(l)} = 2\pi f_i(m,t')\frac{d_l}{c}\sin\theta_i = 2\pi(f_c + \mu t')\frac{d_l}{c}\sin\theta_i, \tag{8}$$

where $\theta_i$ denotes the angle of the $i$th scatterer, $f_i(m, t')$ denotes the instantaneous frequency and is obtained from (7), and $d_l$ denotes the distance between the $l$th element and the reference element, respectively. It is seen in (8) that the phase delay is not only related to the $l$th element, but also the fast-time $t'$. In fact, it is very straightforward because the steering vector is the function of frequency for wideband DOA and the frequency is the function of time for FMCW signal, therefore, the steering vector is also a function of time. Then, the wideband DOA can be transformed into an additional second-order coupling between the indices of elements and the indices of fast-time. Most approaches for joint estimation DOA and Doppler have failed to provide a solution for this wideband DOA estimation [14,26,27]. Besides, the conventional ISSM or CSSM for wideband DOA can be avoided by solving the problem of coupling terms.

In this paper, the targets are located in the far-field and the observation time in one CPI is very short, thus, the angles are assumed not changing in one CPI. Without losing generality, the uniformly distributed linear array (ULA) with omnidirectional elements is used to establish the signal model in the following, where $d_l = ld$ and $d$ is the interspace between the neighbouring elements.

The received signal is then cross-correlated with the transmitted signal and the de-chirped signal of the $i$th scatterer received by $l$th element can be written as

$$\begin{aligned} r_i^{(l)}(m,t)s^*(m,t) &= \alpha_i \exp(j\varphi_i^{(l)}) \exp\left(j2\pi\phi_i(m,t')\right)s^*(m,t') \\ &= \alpha_i \exp(j\varphi_i^{(l)}) \times \\ &\quad \exp\left[-j2\pi\left(f_c\tau_i(m,t') - 0.5\mu\tau_i^2(m,t')\right.\right. \\ &\quad \left.\left. + \mu t'\tau_i(m,t')\right)\right] \\ &\approx \alpha_i \exp(j\varphi_i^{(l)}) \exp\left[-j2\pi\left(f_c\tau_i(m,t')\right.\right. \\ &\quad \left.\left. + \mu t'\tau_i(m,t')\right)\right]. \end{aligned} \tag{9}$$

Substitution of Eq. (4) in the result of Eq. (9) yields the de-chirped data $z_i^{(l)}(m,t)$ given by,

$$\begin{aligned} z_i^{(l)}(m,t') &= \alpha_i \exp(j\varphi_i^{(l)}) \times \exp\left[-j2\pi\left(f_c(\gamma_i + \frac{2v_i}{c}(t'+mT))\right.\right. \\ &\quad \left.\left. + \mu t'(\gamma_i + \frac{2v_i}{c}(t'+mT))\right)\right] \\ &\approx \alpha_i' \exp(j\varphi_i^{(l)}) \exp\left[-j2\pi\left(\mu\gamma_i t' + f_{d,i}Tm\right.\right. \\ &\quad \left.\left. + \mu\frac{2v_i}{c}Tmt'\right)\right], \end{aligned} \tag{10}$$

where $f_{d,i} = \frac{2v_i f_c}{c}$ represents the Doppler frequency of the $i$th scatterer and $\exp(j2\pi f_c\gamma_i)$ is absorbed into $\alpha_i'$ (for simplicity, $\alpha_i$ is still used in the following), and the terms $f_{d,i}t'$ and $\mu\frac{2v_i}{c}t'^2$ are omitted as they are very small. As we can see from (10), the signal model is a 2D complex sinusoid with a coupling term between the fast-time $t'$ and the slow-time number $m$. If the scatterers migrate one or several range bins in one CPI as

$$v_i \times MT \geqslant \frac{c}{2B}, \tag{11}$$

where $MT$ is one CPI formed by $M$ chirps and $v_i$ is the velocity of the $i$th targets. It is called range migration in GMTI and this coupling term will decrease the performance of estimation applying classic Fourier transform. It is worth noting that, the definition of conventional range migration, which shown as a coupling term in the signal model, is based on the Rayleigh criterion. However, the resolution of subspace-based methods has broken the Rayleigh criterion and the coupling terms will always decrease the performance of these methods more or less even if the targets migrate less than one range resolution cell in one CPI.

After the de-chirping, the data in Eq. (10) is sampled with respect to fast-time with frequency $f_s$ and the discretized data $\hat{z}_i^{(l)}$ in the time domain is obtained as

$$\begin{aligned} \hat{z}_i^{(l)}(m,k) &= \alpha_i a^{(l)}(\theta_i) \times \exp\left[-j2\pi\left(-\mu\frac{kld}{cf_s}\sin\theta_i + \mu\gamma_i\frac{k}{f_s}\right.\right. \\ &\quad \left.\left. + f_{d,i}Tm + \mu\frac{2v_i}{cf_s}Tmk\right)\right], \end{aligned} \tag{12}$$

where

$$a^{(l)}(\theta_i) = \exp\left(j2\pi\frac{ld}{\lambda}\sin\theta_i\right), \tag{13}$$

and $\lambda = c/f_c$ is the wavelength of the starting frequency, $k$ denotes the sampling index ($k = 0, 1 \ldots, K-1$, in which $K$ is the total number of snapshots in one chirp). By stacking all the $\hat{z}^{(l)}(m,k)$, the raw data of the $l$th element is written in the matrix format $\mathbf{Z}_i^{(l)} \in \mathbb{C}^{M\times K}$ conform

$$\mathbf{Z}_i^{(l)} = \alpha_i a^{(l)}(\theta_i)(\mathbf{1}_M[\mathbf{h}_i^{(l)}]^T) \odot (\mathbf{f}_{d,i}\mathbf{f}_{r,i}^T) \odot \mathbf{\Phi}_i, \tag{14}$$

where $\mathbf{h}_i^{(l)} \in \mathbb{C}^{K\times 1}$, $\mathbf{f}_{r,i} \in \mathbb{C}^{K\times 1}$ and $\mathbf{f}_{d,i} \in \mathbb{C}^{M\times 1}$ are denoted by

$$\mathbf{h}_i^{(l)} = \left[1, e^{j2\pi\mu\frac{ld}{cf_s}\sin\theta_i}, \ldots, e^{j2\pi\mu\frac{(K-1)ld}{cf_s}\sin\theta_i}\right]^T,$$
$$\mathbf{f}_{r,i} = \left[1, e^{-j2\pi\mu\frac{\gamma_i}{f_s}}, \ldots, e^{-j2\pi\mu\frac{\gamma_i}{f_s}(K-1)}\right]^T,$$
$$\mathbf{f}_{d,i} = \left[1, e^{-j2\pi f_{d,i}T}, \ldots, e^{-j2\pi f_{d,i}T(M-1)}\right]^T, \quad (15)$$

and $\mathbf{\Phi}_i \in \mathbb{C}^{M\times K}$ is denoted by

$$\mathbf{\Phi}_i = \begin{pmatrix} \mathbf{g}_i^T(0) \\ \mathbf{g}_i^T(1) \\ \vdots \\ \mathbf{g}_i^T(M-1) \end{pmatrix}, \quad (16)$$

in which $\mathbf{g}_i(m) \in \mathbb{C}^{K\times 1}$ is given by

$$\mathbf{g}_i(m) = [1, e^{-j2\pi\mu\frac{2v_i}{cf_s}Tm}, \ldots, e^{-j2\pi\mu\frac{2v_i}{cf_s}Tm(K-1)}]^T. \quad (17)$$

The coupling term $\mathbf{1}_M[\mathbf{h}_i^{(l)}]^T$ in Eq. (14) between element indices and fast-time sampling indices is introduced by wideband modulated frequencies. If we consider a narrowband signal, then the signal model reduces to

$$\mathbf{Z}_i^{(l)} = \alpha_i a^{(l)}(\theta_i)\mathbf{f}_{d,i}\mathbf{f}_{r,i}^T. \quad (18)$$

However, the coupling terms are in general too large to be neglected for (Ultra-)WB signals, which we will consider in the following sections. The received signal model $\mathbf{X}^{(l)} \in \mathbb{C}^{M\times K}$ for multiple scatterers in the presence of white Gaussian noise is represented by

$$\mathbf{X}^{(l)} = \sum_{i=1}^{I}\mathbf{Z}_i^{(l)} + \mathbf{N}^{(l)}, \quad (19)$$

where $\mathbf{N}^{(l)} \in \mathbb{C}^{M\times K}$ denotes the Gaussian noise with distribution $\mathcal{CN}(\mathbf{0}, \sigma^2\mathbf{I})$.

### 2.2. Unambiguous angle and velocity

According to the Nyquist sampling criteria, in the sampled dechirped data in Eq. (13) the following parameters are bounded by

$$2\pi T f_{d,i} \in (-\pi, \pi),$$
$$2\pi f_c\frac{d}{c}\sin\theta_i \in (-\pi, \pi), \quad (20)$$

so the unambiguous velocity and angle are obtained as

$$v_m = \frac{c}{4Tf_c},$$
$$\sin(\theta_m) = \min\left\{\frac{c}{2f_c d}, 1\right\}. \quad (21)$$

If the velocities or angles are greater than the unambiguous ones, they will be folded into the unambiguous domain.

## 3. 2D MUSIC algorithm and compensation method

In this section, the classic 2D MUSIC algorithm for joint estimation of DOA and Doppler is presented at first. However, the coupling terms decline the performance of the classic 2D MUSIC, in order to circumvent this a novel compensation method is proposed in the MUSIC algorithm to remove such interference. The estimation of the model order is discussed at last in this section.

### 3.1. 2D MUSIC algorithm

With the three-dimensional signal model, it is possible to apply the MUSIC algorithm for joint parameter estimation if we ignore the coupling terms. Using one dimension of sinusoidal data as reference, the 2D MUSIC algorithm can be implemented for joint two-dimensional parameter estimation. The 3D MUSIC algorithm can be further used for joint three-dimensional parameter estimation for DOA, range and Doppler. The noise subspace can be extracted by applying a spatial smoothing technique to eliminate coherence between the sources [28] or by applying a high order singular value decomposition (HOSVD) [29]. However, it is both time- and memory-consuming to directly apply the 3D MUSIC algorithm. Thus, the 2D MUSIC algorithm is applied here, for instance, to estimate Doppler and DOA jointly. It is worth noting that, the proposed methods can also be applied for joint estimation of Doppler and range or DOA and range. To apply the 2D MUSIC algorithm, the raw data have to be reshaped from the 3-dimensional tensor form to the 2-dimensional matrix form $\mathbf{Y} \in \mathbb{C}^{LM\times K}$ by stacking element and slow-time dimensions together as

$$\mathbf{Y} = \begin{pmatrix} \mathbf{X}^{(0)} \\ \mathbf{X}^{(1)} \\ \vdots \\ \mathbf{X}^{(L-1)} \end{pmatrix}. \quad (22)$$

For simplicity, $\mathbf{Y}$ is rewritten in matrix notation as:

$$\mathbf{Y} = \sum_{i}^{I}\alpha_i(\mathbf{a}_{\theta_i}\otimes\mathbf{f}_{d,i})(\mathbf{f}_{r,i})^T \odot \mathbf{\Omega}_{dr,i} \odot \mathbf{\Omega}_{\theta r,i} + \mathbf{N}, \quad (23)$$

where $\mathbf{a}_{\theta_i} \in \mathbb{C}^{L\times 1}$, $\mathbf{\Omega}_{dr,i} \in \mathbb{C}^{LM\times K}$ and $\mathbf{\Omega}_{\theta r,i} \in \mathbb{C}^{LM\times K}$ are given by,

$$\mathbf{a}_{\theta_i} = [1, a^{(1)}(\theta_i), \ldots, a^{(L-1)}(\theta_i)]^T,$$
$$\mathbf{\Omega}_{dr,i} = \mathbf{1}_L \otimes \mathbf{\Phi}_i,$$
$$\mathbf{\Omega}_{\theta r,i} = \begin{pmatrix} (\mathbf{h}_i^{(0)})^T \\ (\mathbf{h}_i^{(1)})^T \\ \vdots \\ (\mathbf{h}_i^{(L-1)})^T \end{pmatrix} \otimes \mathbf{1}_M. \quad (24)$$

Now, the classic 2D MUSIC algorithm is applied directly by ignoring the coupling terms. First, the covariance matrix $\mathbf{R} \in \mathbb{C}^{LM\times LM}$ is computed according to

$$\mathbf{R} = \mathbb{E}(\mathbf{Y}\mathbf{Y}^H). \quad (25)$$

The eigendecomposition is applied to split the data space into the noise subspace associated to the noise eigenvectors $\mathbf{U_n}$ and the signal subspace associated to the signal eigenvectors $\mathbf{U_s}$.

$$\mathbf{R} = \mathbf{U}\mathbf{\Lambda}\mathbf{U}^H,$$
$$\mathbf{U} = [\mathbf{U_s}\ \mathbf{U_n}]. \quad (26)$$

To extract the noise subspace we assume that the number of scatterers is known. The estimation of the number of scatterers will be discussed later. The matched steering vector $\boldsymbol{\alpha}(v_p, \theta_q) \in \mathbb{C}^{LM\times 1}$ for the velocity $v_p$ and the angle $\theta_q$ is formulated as:

$$\boldsymbol{\alpha}(v_p, \theta_q) = \mathbf{a}_{\theta_q}\otimes\mathbf{f}_{d,p}. \quad (27)$$

After that, the MUSIC spectrum at the point $(v_p, \theta_q)$ can be calculated by

$$P(v_p, \theta_q) = \frac{1}{\boldsymbol{\alpha}^H(v_p, \theta_q)\mathbf{U_n}\mathbf{U_n}^H\boldsymbol{\alpha}(v_p, \theta_q)}. \quad (28)$$

### 3.2. Compensation for coupling terms

Directly applying the classic MUSIC algorithm without any phase compensation yields an estimation performance that is significantly less accurate due to the influence of the coupling terms. Hence, phase adjustment is needed before the MUSIC algorithm is

applied. Although the Keystone transform is the most common approach for the coupling term adjustment, the interpolation of the Keystone transform leads to significant phase errors when the data size is small [18,30]. Despite this drawback, the performance of Keystone transform will be discussed and compared with the proposed algorithm in Section 5. Fortunately, since the coupling terms are functions of $v$ for $\mathbf{\Omega}_{dr,i}$ and $\theta$ for $\mathbf{\Omega}_{\theta r,i}$, we are able to remove the coupling terms in each scanning grid. The compensation term for the grid in terms of $(v_p, \theta_q)$ is formulated as

$$\mathbf{C} = (\mathbf{\Omega}_{dr,p} \odot \mathbf{\Omega}_{\theta r,q})^*. \tag{29}$$

Then by Hadamard product with the raw data matrix $\mathbf{Y}$ yields

$$\hat{\mathbf{Y}} = \mathbf{Y} \odot \mathbf{C}. \tag{30}$$

Since the compensation term is just a phase shift, it will not increase the noise power. The coupling terms of the new obtained data are removed for the grid in terms of $(v_p, \theta_q)$. With this compensation, not only the phase is adjusted to improve the accuracy, but also the orthogonality between the steering vector and the noise subspace is enhanced which helps to improve the resolution. The covariance matrix is calculated using the improved data $\hat{\mathbf{Y}}$ according to

$$\hat{\mathbf{R}} = E(\hat{\mathbf{Y}}\hat{\mathbf{Y}}^H). \tag{31}$$

Finally, the 2D MUSIC algorithm (28) can be applied to the improved covariance matrix. The algorithm is concluded in Algorithm 1.

**Algorithm 1** 2D MUSIC with Compensation.

Reshape the raw data as (22)
**for** $v_p$ in $[-v_m, v_m]$ **do**
  **for** $\theta_q$ in $[-\theta_m, \theta_m]$ **do**
    $\mathbf{C} := (\mathbf{\Omega}_{dr,p} \odot \mathbf{\Omega}_{\theta r,q})^*$
    $\hat{\mathbf{Y}} := \mathbf{Y} \odot \mathbf{C}$
    $\hat{\mathbf{R}} := \mathbb{E}(\hat{\mathbf{Y}}\hat{\mathbf{Y}}^H)$
    $\hat{\mathbf{R}} =: \mathbf{U}\mathbf{\Lambda}\mathbf{U}^{-1}$ # Eigendecomposition
    $\mathbf{U_n} := \mathbf{U}[:, I : end]$
    $\boldsymbol{\alpha}(v_p, \theta_q) := \mathbf{a}_{\theta_q} \otimes \mathbf{f}_{d,p}$
    $P(v_p, \theta_q) := \dfrac{1}{\boldsymbol{\alpha}^H(v_p, \theta_q)\mathbf{U_n}\mathbf{U_n}^H\boldsymbol{\alpha}(v_p, \theta_q)}$
  **endfor**
**endfor**

### 3.3. Estimation of the target number

Before implementing the 2D MUSIC algorithm, the number of targets has to be estimated to correctly split the noise subspace. Apparently, the coupling terms in the UWB signal model bring difficulties to estimate the number of the targets, since the eigenvalues decrease more smoothly than that of narrowband data. Therefore, a method is proposed for the estimation of the number of targets involved. Usually, the number of targets is much smaller

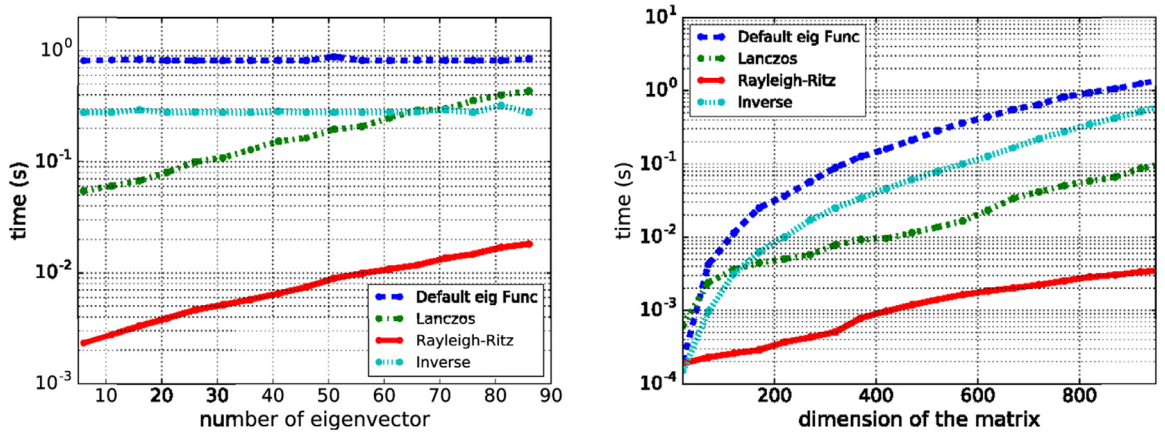


**Fig. 1.** Time consumption comparison for (a) calculating the different number of eigenvectors with the same dimension of the Hermitian matrix of $768 \times 768$ and (b) calculating 10 eigenvectors with the different dimension of the Hermitian matrix.

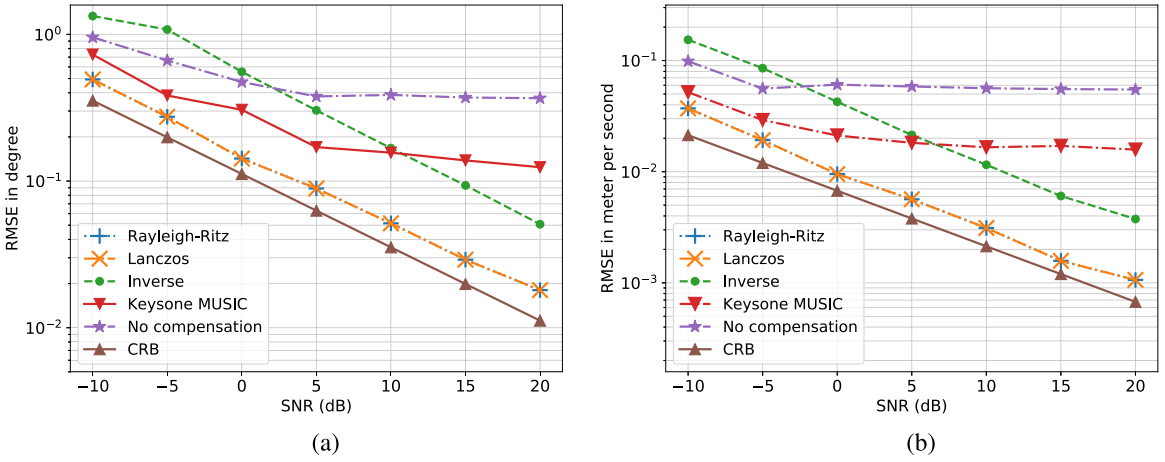


**Fig. 2.** Comparison of RMSEs with CRLB as a function of SNR at $B = 1$ GHz for one target at angle 40° and velocity 8 m/s. (a) angle estimation and (b) velocity estimation.

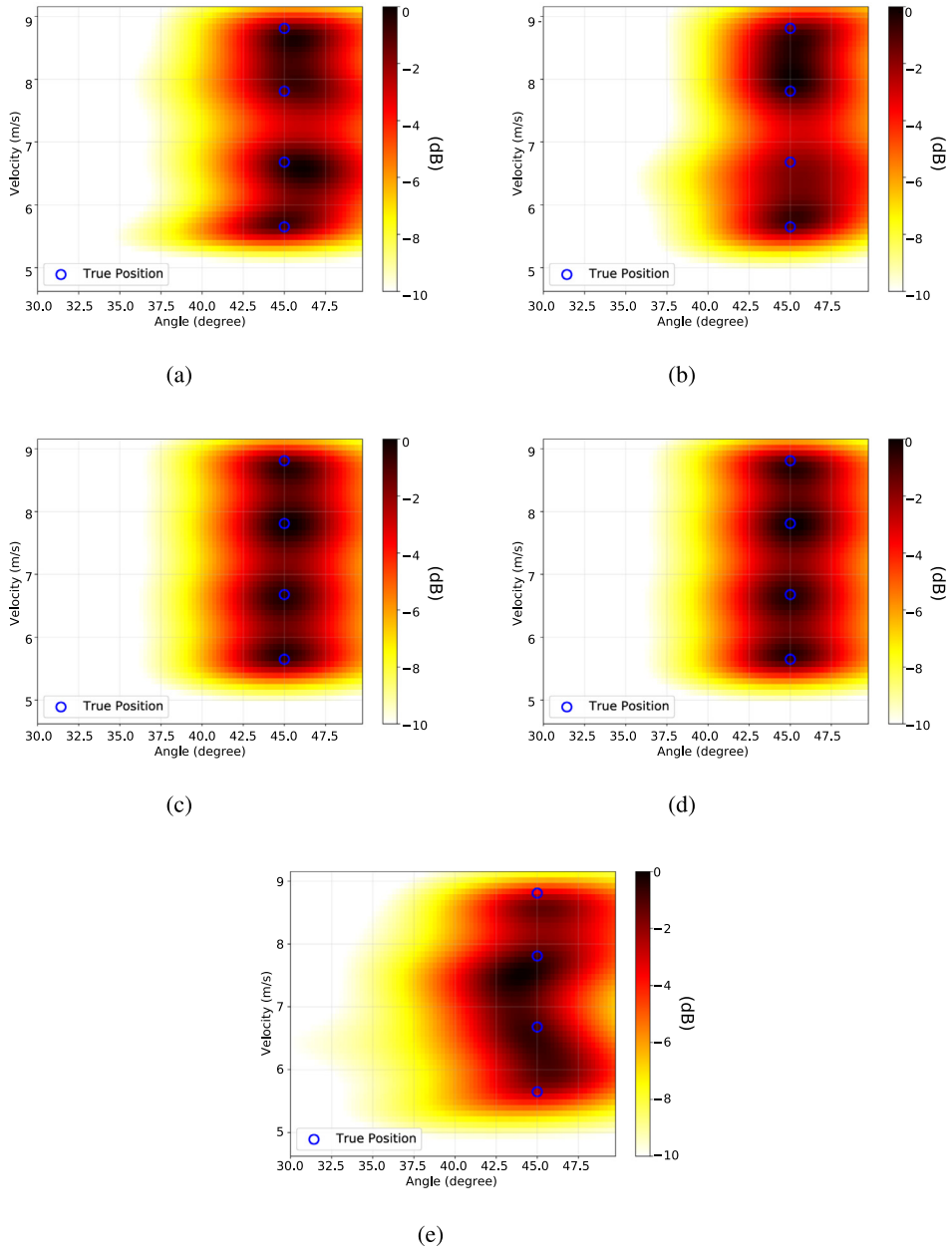


**Fig. 3.** Angle-Velocity maps of $B = 1$ GHz and $SNR = 3$ dB for (a) 2D MUSIC without phase compensation, (b) 2D MUSIC after Keystone transform, (c) 2D MUSIC with phase compensation and accelerated by Lanczos algorithm, (d) 2D MUSIC with phase compensation and accelerated by Rayleigh–Ritz step and (e) 2D MUSIC with phase compensation and accelerated by inverse algorithm.

than the dimension of the covariance matrix, so the dimension of the signal subspace is allowed to be slightly overestimated. According to this property, a larger model order than the true one can be selected at first to image the MUSIC pseudo-spectrum. Then by using peaks detection methods, we estimate the number of the targets from the MUSIC pseudo-spectrum. Although it is allowed to assume the larger dimension of the signal subspace than the true one, it provides better imaging results by using the whole noise subspace. After we obtain the number of targets, the proposed algorithms can be applied to obtain better estimations. The simulations of such a method will be shown in Section 5.3.

## 4. Efficient implementation

In this section, the efficient implementations of the proposed method are proposed by accelerating the extraction of the noise subspace and parallel implementation.

### 4.1. Efficient implementation for the noise subspace extraction

As for 2D MUSIC, the dimension of the covariance matrix $LM \times LM$ is usually very large. Thus, it is a heavy computational burden to perform all the eigendecompositions for each scanning grid and limits the proposed methods for real applications. Fortunately, as the covariance is a Hermitian matrix, some properties of the algorithm allow opportunities to accelerate the algorithm. The first one is that the number of targets is usually much smaller than the dimension of the covariance matrix. Instead of calculating all eigenvectors, one can only calculate the needed eigenvectors in the signal subspace, while the noise subspace can be easily obtained from the orthogonal complement subspace of the signal subspace according to,

$$\mathbf{U_n}\mathbf{U_n}^H = \mathbf{I} - \mathbf{U_s}\mathbf{U_s}^H. \tag{32}$$

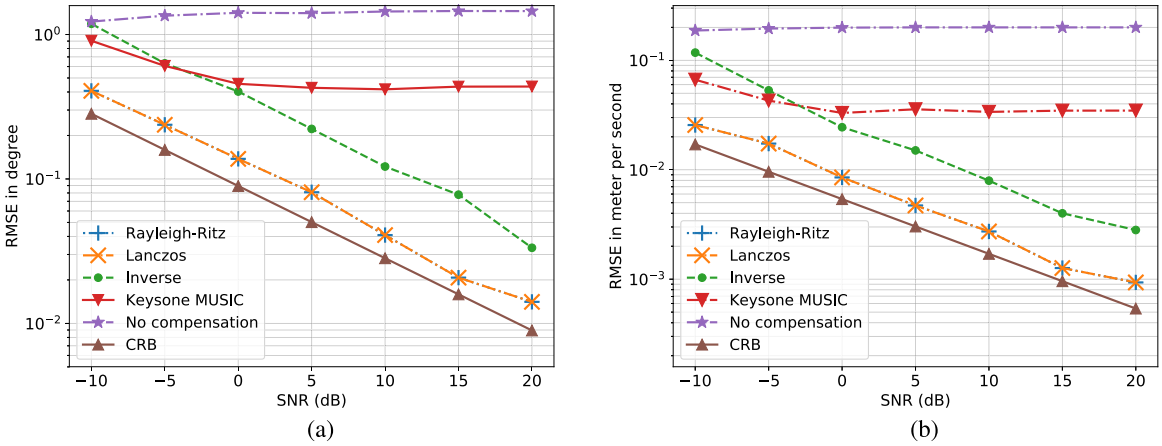


**Fig. 4.** Comparison of RMSEs with CRLB as a function of SNR at $B = 4$ GHz for one target at angle 40° and velocity 8 m/s. (a) angle estimation and (b) velocity estimation.

Another interesting property is that the compensation term is just a minor phase shift. Therefore, the signal subspaces in each adjacent grid are close to each other in the norm. Based on these properties, two acceleration methods are introduced, namely the Lanczos algorithm and the Rayleigh-Ritz step. The inverse approach in [26] is also mentioned for comparison.

#### 4.1.1. Lanczos algorithm

The Lanczos algorithm is an iterative method for calculating the eigendecomposition of large Hermitian/symmetric matrix [31]. It saves a lot of computation by only computing the largest eigenvalues and their corresponding eigenvectors. Thus, it can be used in scenarios where only the signal subspace is needed and the dimension of the signal subspace is much smaller than that of the covariance matrix.

#### 4.1.2. Rayleigh–Ritz step

Lanczos is much faster to extract the signal subspace than the default *eig* function if the dimension of the signal subspace is small. However, it is not fast enough and we do not take advantage of the fact that the adjacent signal subspaces are close to each other. The signal subspaces for neighbouring grids are close to each other in the norm so the previous signal subspace provides a good initial guess to calculate the next one. Thus, the Rayleigh–Ritz step method [32] is adopted to use the previous signal subspace as the initial guess to approach the current signal subspace. According to the simulation, just one step is needed to obtain a sufficiently good eigenvector approximation.

#### 4.1.3. Inverse algorithm without EVD

In [26], the authors propose to use the inverse of the covariance matrix to replace the noise subspace. Certainly, calculating the inverse or pseudo-inverse of a huge matrix will save a lot of time compared to calculating the eigendecomposition. It shows comparable results with MUSIC but is faster than eigendecomposition MUSIC. However, this method can only work in high SNR condition. If the SNR is low, the approximation of this method no longer valid. Besides, the convergence performance of matrix inverse/pseudo-inverse is not monotonically increasing with the snapshot/SNR [33]. Thus this algorithm is not stable and robust. Despite its disadvantages, from the computational burden and estimation performance perspectives, we use this algorithm as a reference to compare it with our proposed algorithms.

#### 4.1.4. Comparison

To compare the priority of selected methods on time consumption, we first fix the dimension of the covariance matrix and simulate the time consumption with the different number of eigenvectors associated with the largest eigenvalues. The simulation results with a mean time of 100 repeats using Python3.5 with SciPy0.19 under Inter(R) Core i5-6500 @ 3.20 GHz are shown in Fig. 1(a). (It is worth noting that the results using MATLAB could be different.)

The time consumption is not only influenced by the number of eigenvectors associated with the largest eigenvalues, but also by the dimension of the covariance matrix. Thus, the comparison of time consumption with the different dimensions of the covariance matrix is shown in Fig. 1(b). As we can see, the time consumption of the default *eig* function increases significantly with the dimension of the covariance matrix as it needs $\mathcal{O}(n^3)$ flops (float number operations). The Rayleigh-Ritz step shows to be the most efficient method among all of them.

The computational complexity is shown in Table 1, where $n$ represents the dimension of the Hermitian matrix and $\beta$ represents the number of eigenvectors associated with the $\beta$ largest eigenvalues.

According to the above analysis, using the Rayleigh-Ritz step as an example, the algorithm can be illustrated as Algorithm 2.

**Algorithm 2** Compensation algorithm with Rayleigh–Ritz step.

Reshape the raw data $\mathbf{Y}$ as (22)
$\mathbf{R} := \mathbb{E}(\mathbf{Y}\mathbf{Y}^H)$
$\mathbf{R} =: \mathbf{U}\mathbf{\Lambda}\mathbf{U}^H$ # Eigendecomposition
$\mathbf{U_s} := \mathbf{U}[:, 0 : I-1]$
**for** $\nu_p$ in $[-\nu_m, \nu_m]$ **do**
  $\hat{\mathbf{Y}} := \mathbf{Y} \odot (\mathbf{\Omega}_{dr,p})^*$
  **for** $\theta_q$ in $[-\theta_m, \theta_m]$ **do**
    $\hat{\mathbf{Y}} := \hat{\mathbf{Y}} \odot (\mathbf{\Omega}_{\theta r,q})^*$
    $\hat{\mathbf{R}} := \mathbb{E}(\hat{\mathbf{Y}}\hat{\mathbf{Y}}^H)$
    $\mathbf{Z} := \hat{\mathbf{R}}\mathbf{U_s}$
    $\mathbf{Z} =: \mathbf{Q}\mathbf{P}$ # QR decomposition
    $\mathbf{H} := \mathbf{Q}^H\hat{\mathbf{R}}\mathbf{Q}$
    $\mathbf{H} =: \mathbf{F}\mathbf{\Theta}\mathbf{F}^H$ # Eigendecomposition
    $\mathbf{U_s} := \mathbf{Q}\mathbf{F}$
    $\boldsymbol{\alpha}(\nu_p, \theta_q) := \mathbf{a}_{\theta_q} \otimes \mathbf{f}_{d,p}$
    $P(\nu_p, \theta_q) := \dfrac{1}{\boldsymbol{\alpha}^H(\nu_p, \theta_q)(\mathbf{I} - \mathbf{U_s}\mathbf{U_s}^H)\boldsymbol{\alpha}(\nu_p, \theta_q)}$
  **endfor**
**endfor**

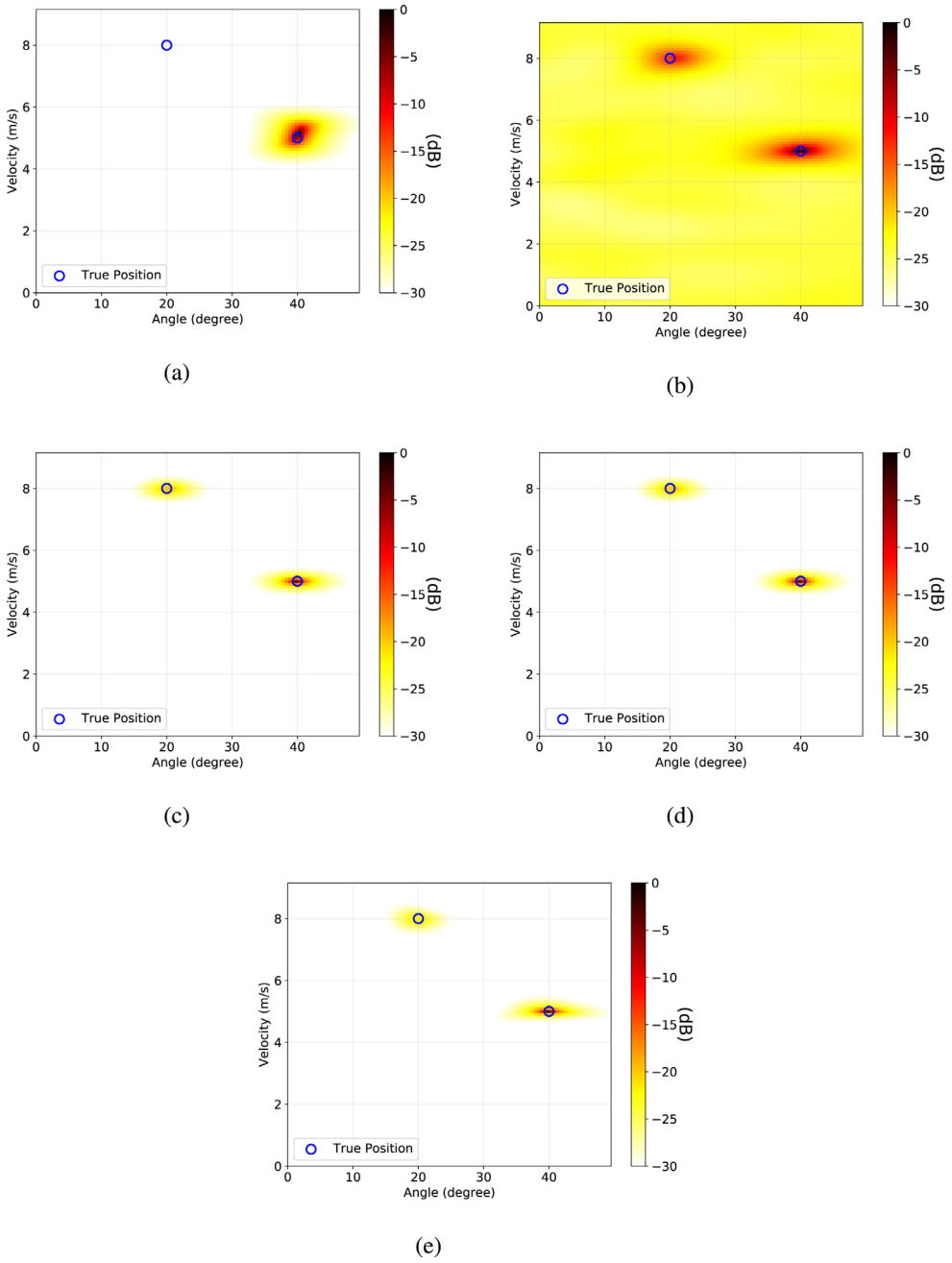


**Fig. 5.** Angle-Velocity maps of $B = 4$ GHz and $SNR = 30$ dB for (a) 2D MUSIC without phase compensation, (b) 2D MUSIC after Keystone transform, (c) 2D MUSIC with phase compensation and accelerated by Lanczos algorithm, (d) 2D MUSIC with phase compensation and accelerated by Rayleigh–Ritz step and (e) 2D MUSIC with phase compensation and accelerated by inverse algorithm.

### 4.2. Parallel processing

As the 2D MUSIC algorithm is a scanning process, it is possible to divide the scanning domain into several parts related to CPU cores for parallel processing. We can process each part parallelly to fully utilize the hardware. Here, by using a *threading* package in python3.5, we divide the scanning domain into 4 parts with identical size and by using covariance matrix size of $256 \times 256$, the computational time with and without parallel computing are 25.8 s and 41.9 s, respectively. In the simulation, 62% of the computational time is saved by using parallel processing.

## 5. Simulations

In this section, the performance of the proposed methods is discussed. As the coupling terms are related to the bandwidth, the performance of the proposed methods with different bandwidths, i.e. 1 GHz and 4 GHz, will be simulated. The system parameters used for simulation are shown in Table 2.

### 5.1. Bandwidth 1 GHz

We start with considering a case with a bandwidth of $B = 1$ GHz, where the relative bandwidth is 1.3%. Fig. 2 shows the

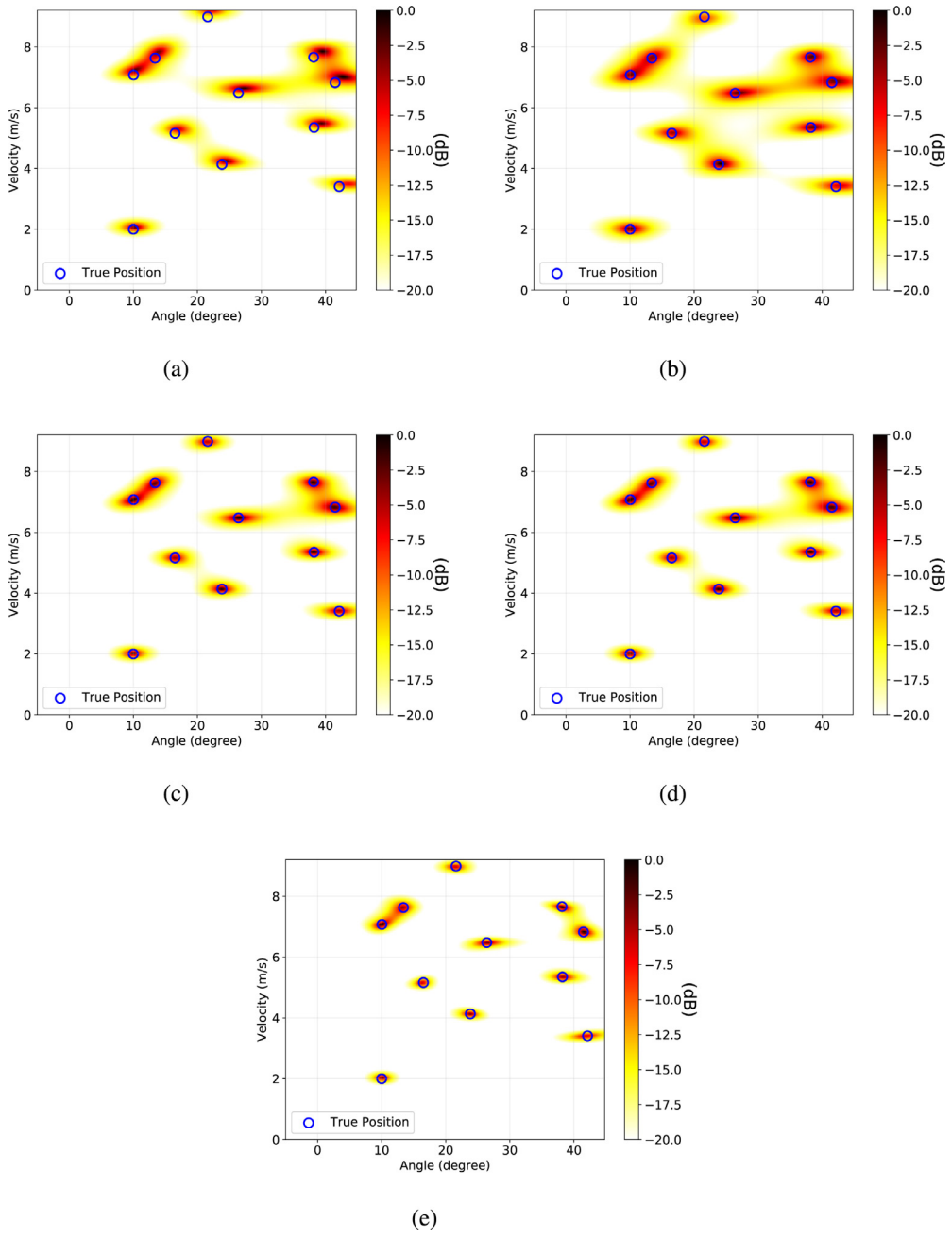


**Fig. 6.** Angle-Velocity maps of $B = 4$ GHz and $SNR = 20$ dB for (a) 2D MUSIC without phase compensation, (b) 2D MUSIC after Keystone transform, (c) 2D MUSIC with phase compensation and accelerated by Lanczos algorithm, (d) 2D MUSIC with phase compensation and accelerated by Rayleigh–Ritz step and (e) 2D MUSIC with phase compensation and accelerated by inverse algorithm.

**Table 1**
Computational complexity.

| Algorithm | Computational complexity |
|---|---|
| Default *eig* Func | $\mathcal{O}(n^3)$ |
| Inverse | $\mathcal{O}(\frac{1}{3}n^3)$ |
| Lanczos | $\mathcal{O}(\beta n^2)$ |
| Rayleigh-Ritz | $\mathcal{O}(\beta^2 n + \beta^3)$ |

**Table 2**
Parameters of system.

| Parameters | Value |
|---|---|
| Number of Chirps in one CPI | 16 |
| Number of Snapshots in one Chirp | 32 |
| Number of Antenna Elements | 8 |
| Starting Frequency | 77 GHz |
| Inter-element Distance | 1.899 mm |
| Chirp Repetition Interval | 0.1 ms |
| Chirp Duration | 0.09 ms |

root-mean-square errors (RMSEs) of estimates of DOA and Doppler of a single point scatterer with the radial velocity 8 m/s, angle 40° and range 80 m as a function of the SNR. They are compared with the corresponding Cramér-Rao lower bounds (CRLB) (see Appendix for CRLB derivation). The RMSEs are obtained from 40 Monte Carlo trials. As classic MUSIC is a biased estimator, the RMSEs will not decrease with an increase of SNR. One can also observe that the RMSEs of the Keystone MUSIC do not always decrease along with

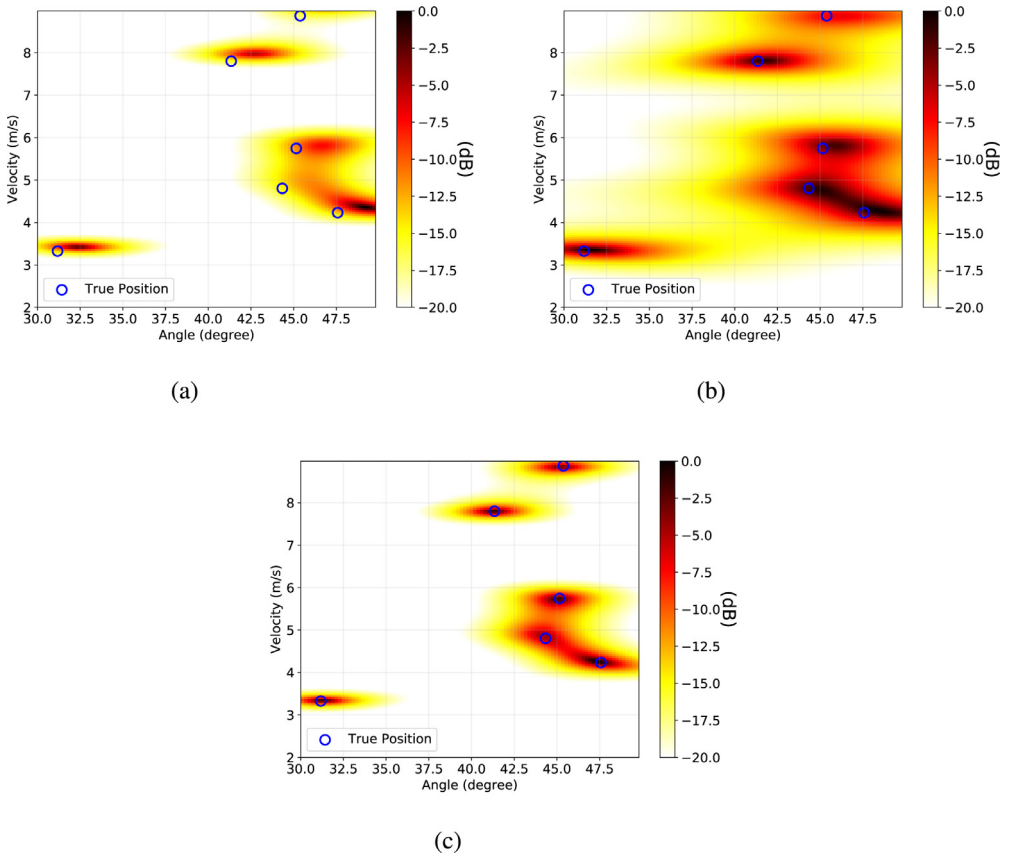


**Fig. 7.** (a) 2D MUSIC without phase compensation and (b) 2D MUSIC after Keystone transform (c) 2D MUSIC with phase compensation and accelerated by Rayleigh–Ritz step.

**Table 3**
Comparison of computational time.

| Algorithm | Computational Time |
|---|---|
| Default *eig* Func | 152.68 s |
| Lanczos | 18.75 s |
| Rayleigh-Ritz | 5.48 s |
| Inverse | 32.66 s |
| Keystone MUSIC | 1.01 s |

the increase of the SNR since the error introduced by the interpolation will dominantly decrease the accuracy of the estimation at high SNR condition.

We further focus on the performance of the proposed methods in a challenging scenario. To this end, four closely positioned point scatterers with the same angles $\theta = 45^\circ$ and the same amplitudes 0 dB, but close radial velocities $v = [4.6, 5.68, 6.86, 7.91]$ m/s and random range from 100 m to 200 m are set. The SNR is set to 3 dB. The normalized results are shown in Fig. 3. While the inverse method and the classic MUSIC algorithm without phase compensation are not able to separate scatterers from each other, MUSIC with phase compensation (in both Lanczos and Rayleigh–Ritz acceleration implementations) achieves at least -3 dB isolation between the scatterers. The Keystone-MUSIC (Fig. 3(b)) shows some separation of the scatterers with low speed, but fast-moving scatterers are not separated. Table 3 shows the time consumptions of the four methods and the compensated MUSIC algorithm with default *eig* function, where the observation domain is divided into a $100 \times 100$ grid. It is worth noting that the superiority with respect to the computational time of the proposed algorithm could be more significant if the dimension of the covariance matrix is larger.

### 5.2. Bandwidth 4 GHz

Next, we increase the bandwidth from 1 GHz to 4 GHz, where the relative bandwidth is 5.1%. According to the model from (23), the estimation accuracy will deteriorate as the bandwidth increases. The same point scatterer with radial velocity 8 m/s, angle 40° and range 80 m is set for RMSE simulation. The obtained RMSEs results of the proposed methods and the competitors are compared with CRLB in Fig. 4. The error of the no compensation method is much larger than what we obtained in the case of $B = 1$ GHz.

The next simulation is to test the ability of the proposed algorithm to detect a relatively weak target. According to the analysis, if there is a strong migrated target present in an observation domain, the energy of this target will dominantly spread into several eigenvectors. Thus, the subspace corresponding to the relatively weak target will be allocated to noise subspace. Two targets, one with range 100 m, angle 20°, velocity 8 m/s and amplitude $\alpha = -10$ dB and another one with range 80 m, angle 40°, radial velocity 5 m/s and amplitude $\alpha = 0$ dB, are set. The SNR is set to 30 dB. The results are shown in Fig. 5, where for improved visibility the results are normalized. From Fig. 5(a), we can see that the weak target is missing in the classic MUSIC result without phase compensation. Both targets are seen in the MUSIC pseudo-spectrum obtained by Keystone MUSIC algorithms, however, the peaks corresponding to the targets are wider than in the conventional MUSIC or proposed algorithms and their relative contrast with the background is much smaller in magnitude.

Then 11 point scatterers with random angles from 0° to 50°, random radial velocities from 0 m/s to 9 m/s and random ranges from 100 m to 200 m random $\alpha$ from $-3$ dB to 0 dB are set and

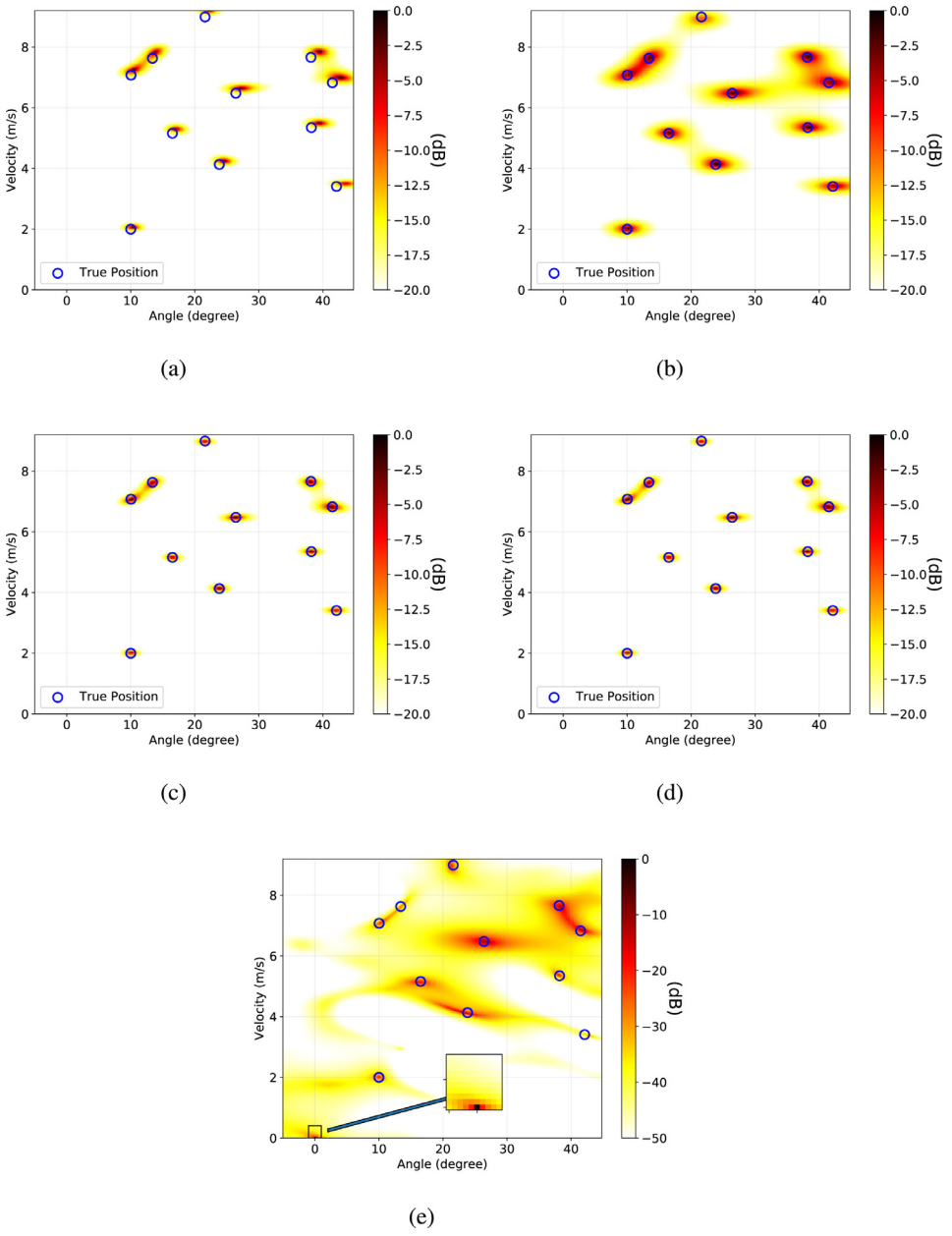


**Fig. 8.** Angle-Velocity maps of $B = 4$ GHz, $SNR = 20$ dB and 128 snapshots for (a) 2D MUSIC without phase compensation, (b) 2D MUSIC after Keystone transform, (c) 2D MUSIC with phase compensation and accelerated by Lanczos algorithm, (d) 2D MUSIC with phase compensation and accelerated by Rayleigh-Ritz step and (e) 2D MUSIC with phase compensation and accelerated by inverse algorithm.

the SNR is set to 20 dB. The normalized results are presented in Fig. 6, where the dynamic range is limited to 20 dB. From the angle-velocity map, one can conclude that the peaks of estimation without phase compensation are biased towards higher velocities and widened (especially in the azimuthal domain) in comparison with that of the proposed methods. Although the accuracies of estimation are slightly better, the Keystone MUSIC suffers from a poor resolution of closely spaced targets (especially in azimuthal domain). At the same time, all three compensation algorithms demonstrate the clear separation of all targets and accurate estimation of their parameters. To show the improvement of the resolution of the proposed compensation method, an extra simulation using the same system parameters of 6 random point targets with large angles and velocities is implemented. The results without compensation, phase adjustment by Keystone transform and phase compensation by the proposed method are presented in Fig. 7. The three closely positioned targets are hardly resolved from Fig. 7(a)(b), while they are clearly resolved in Fig. 7(c).

In the next simulation, we keep the same parameters as before while increase the snapshots from 32 to 128. The results of the 11 point targets from the previous simulation are presented in Fig. 8. The imaging performance of the inverse algorithm significantly degrades when we increase snapshots to 128 and a strong ghost target appears at the position $(v = 0, \theta = 0)$, while the Rayleigh-Ritz and Lanczos algorithms reveal sharper peaks related to targets. It is noted that the results agree with the simulation in [33].

### 5.3. Number of the targets estimation

The 11 point scatterers from the previous simulation are used again in this simulation and the SNR is set to 20 dB. Fig. 9 shows

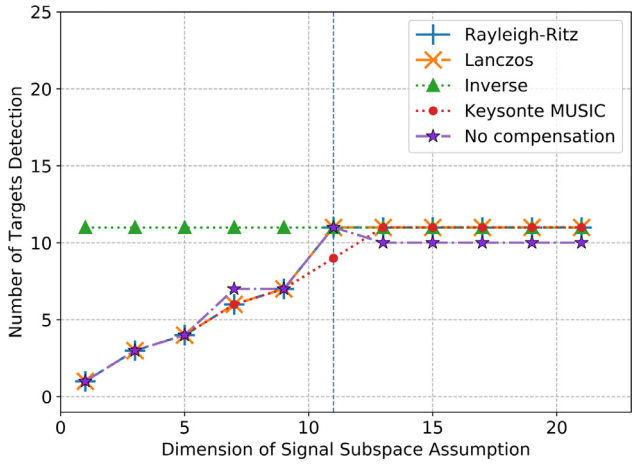


**Fig. 9.** The number of targets estimation from MUSIC pseudo-spectrum using different dimensions of the signal subspace assumptions.

the number of target estimations using the different dimension of the signal subspace assumption. The connected region label algorithm is used here to obtain the number of targets from the binarized MUSIC spectrum. Here the threshold for binarization is set to −7 dB, which is a third of the mean value of the normalized MUSIC spectrum of a large number of target assumptions.

Fig. 10 shows the MUSIC spectrum of Rayleigh-Ritz method and classic MUSIC without compensation for the incorrect dimension of signal subspace assumptions. From the results, both classic MUSIC and compensation MUSIC will miss targets if the dimension of the signal subspace is underestimated. However, compared with Fig. 6, our proposed compensation MUSIC has a higher tolerance for overestimating the dimension of signal subspace than that of classic MUSIC.

## 6. Conclusions

In this paper, a novel joint Doppler-DOA estimation using the UWB FMCW array-based radar for moving targets is proposed. We present an accurate signal model for radar returns from moving targets which at first takes both range migration and wideband DOA into account. Using this model we introduce a modified MUSIC algorithm to eliminate the influence of the intercoupling terms. The method adjusts the phase of the raw data in each scanning grid before eigendecomposition to improve the accuracy of the Doppler and DOA estimation. Moreover, we propose two efficient implementations, namely a Lanczos algorithm and a Rayleigh-Ritz step, to reduce the computational burden specifically for the proposed method.

By comparing RMSEs and CRLB of conventional MUSIC, Keystone MUSIC and proposed algorithm (for the bandwidth of 1GHz and 4GHz) via numerical simulations, we demonstrate that the phase compensation algorithm improves the accuracies of both Doppler and DOA estimation over the conventional and Keystone MUSIC and the accuracies of the proposed algorithm improve with SNR. For example, the accuracies of both Doppler and DOA estimations are improved more than 20 dB for SNR = 20 dB in Fig. 4. Although for SNR below -10dB Keystone MUSIC has accuracy similar to the proposed method, the resolution and overall contrast

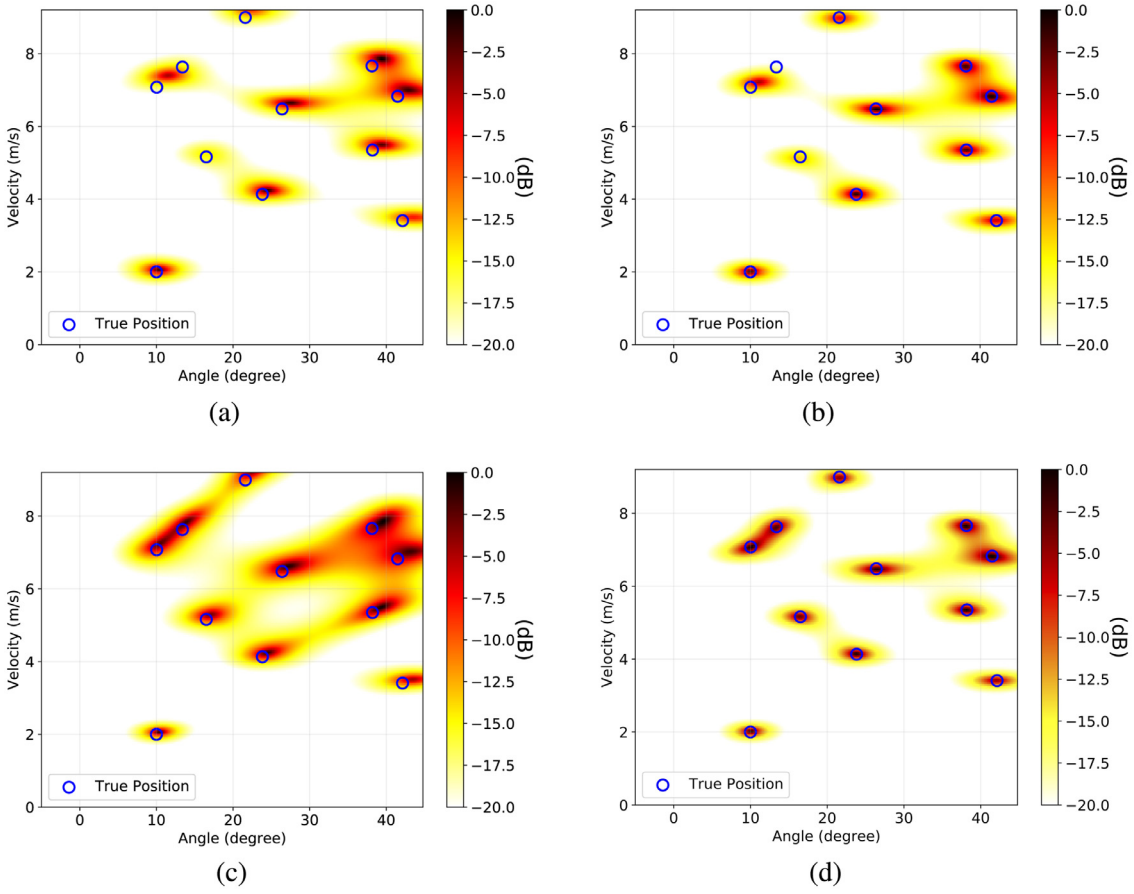


**Fig. 10.** Angle-Velocity maps of $B = 4$ GHz, $SNR = 20$ dB and 32 snapshots for (a) 2D MUSIC without compensation assume 10 targets, (b) Rayleigh–Ritz step assume 10 targets, (c) 2D MUSIC without compensation assume 16 targets and (d) Rayleigh-Ritz step assume 16 targets.

of the MUSIC pseudo-spectrum are worse than by the algorithm proposed. Due to the phase compensation, the algorithm proposed also resolves targets closely spaced in the velocity-angular domain, which are not resolvable both with conventional and Keystone MUSIC algorithms. Further, we show that the proposed Lanczos algorithm and Rayleigh–Ritz are more robust than the inverse algorithm in our simulations. In addition, the Rayleigh–Ritz step shows superiority with respect to computational time when the number of targets is much smaller than the dimension of the signal covariance matrix and has a high tolerance for overestimating the dimension of the signal subspace.

## Declaration of Competing Interest

The authors declare that they have no known competing financial interests or personal relationships that could have appeared to influence the work reported in this paper.

## Acknowledgment

The authors would like to thank the China Scholarship Council (CSC) for the funding support. The authors thank the editor and the anonymous referees for their valuable suggestions and comments.

## Appendix: CRLB derivation

To formulate the CRB matrix, we first reshape the raw data into the vector form $\mathbf{y} \in \mathbb{C}^{LMK\times 1}$ as

$$\mathbf{y} = \sum_{i=1}^{I} \alpha_i (\mathbf{a}_{\theta_i} \otimes \mathbf{f}_{d,i} \otimes \mathbf{f}_{r,i}) \odot \boldsymbol{\omega}_{dr,i} \odot \boldsymbol{\omega}_{\theta r,i} + \mathbf{n}, \tag{33}$$

where $\boldsymbol{\omega}_{dr,i} \in \mathbb{C}^{LMK\times 1}$, $\boldsymbol{\omega}_{\theta r,i} \in \mathbb{C}^{LMK\times 1}$ are

$$\boldsymbol{\omega}_{dr,i} = \mathbf{1}_L \otimes \begin{pmatrix} \mathbf{g}_i(0) \\ \mathbf{g}_i(1) \\ \vdots \\ \mathbf{g}_i(M-1) \end{pmatrix}, \qquad \boldsymbol{\omega}_{\theta r,i} = \begin{pmatrix} \mathbf{1}_M \otimes \mathbf{h}_i^{(0)} \\ \mathbf{1}_M \otimes \mathbf{h}_i^{(1)} \\ \vdots \\ \mathbf{1}_M \otimes \mathbf{h}_i^{(L-1)} \end{pmatrix}. \tag{34}$$

Let $\mathbf{Q} \in \mathbb{C}^{LMK\times 1}$ be the noise covariance matrix, which is

$$\mathbf{Q} = E(\mathbf{n}\mathbf{n}^H) = \sigma^2 \mathbf{I}_{MLK}, \tag{35}$$

with $\sigma^2$ being the variances of the noise. According to the extended Slepian-Bangs' formula [34], the $ij$th element of the fisher information matrix (FIM) has the form:

$$\{\mathrm{FIM}\}_{ij} = \mathrm{Tr}\left(\mathbf{Q}^{-1}\frac{\partial \mathbf{Q}}{\partial \boldsymbol{\eta}_i}\mathbf{Q}^{-1}\frac{\partial \mathbf{Q}}{\partial \boldsymbol{\eta}_j}\right) + 2\Re\left[\left(\frac{\partial \mathbf{y}}{\partial \boldsymbol{\eta}_i}\right)^H \mathbf{Q}^{-1}\left(\frac{\partial \mathbf{y}}{\partial \boldsymbol{\eta}_j}\right)\right], \tag{36}$$

where

$$\boldsymbol{\eta} = [\boldsymbol{\theta}, \mathbf{v}]^T, \tag{37}$$

with $\boldsymbol{\theta}$ and $\mathbf{v}$ being the vectors consisting of the DOAs and Doppler frequencies, respectively. $\partial \mathbf{y}/\partial \boldsymbol{\eta}_i$ denotes the derivative of $\mathbf{y}$ with respect to the $i$th parameter of $\boldsymbol{\eta}$. Note that the FIM is block diagonal since the parameters in $\mathbf{Q}$ are independent of those in $\mu$ and vice versa. Thus, the CRB matrix for the motion parameters can be calculated from the second term on the right side of (36). Let

$$\begin{aligned} \boldsymbol{\chi}_i^{\theta} &= j\xi_{1,i}(\mathbf{d}_L \odot \mathbf{a}_{\theta_i}) \otimes \mathbf{f}_{d,i} \otimes \mathbf{f}_{r,i} \odot \boldsymbol{\omega}_{dr,i} \odot \boldsymbol{\omega}_{\theta r,i} \\ &\quad + j\xi_{2,i}\mathbf{a}_{\theta_i} \otimes \mathbf{f}_{d,i} \otimes \mathbf{f}_{r,i} \odot \boldsymbol{\omega}_{dr,i} \odot [\boldsymbol{\omega}_{\theta r,i} \odot (\mathbf{d}_L \otimes \mathbf{1}_M \otimes \mathbf{d}_K)], \end{aligned} \tag{38}$$

$$\begin{aligned} \boldsymbol{\chi}_i^{\mathbf{v}} &= j\zeta_{1,i}\mathbf{a}_{\theta_i} \otimes (\mathbf{d}_M \odot \mathbf{f}_{d,i}) \otimes \mathbf{f}_{r,i} \odot \boldsymbol{\omega}_{dr,i} \odot \boldsymbol{\omega}_{\theta r,i} \\ &\quad + j\zeta_{2,i}\mathbf{a}_{\theta_i} \otimes \mathbf{f}_{d,i} \otimes \mathbf{f}_{r,i} \odot [(\mathbf{1}_L \otimes \mathbf{d}_M \otimes \mathbf{d}_K) \odot \boldsymbol{\omega}_{dr,i}] \odot \boldsymbol{\omega}_{\theta r,i}, \end{aligned} \tag{39}$$

where $\xi_{1,i} = 2\pi\alpha_i f_c \frac{d}{c}\cos\theta_i$, $\xi_{2,i} = 2\pi\alpha_i \mu \frac{d}{cf_s}\cos\theta_i$, $\zeta_1 = -4\pi\alpha_i T\frac{f_c}{c}$, $\zeta_2 = -4\pi\alpha_i T\frac{\mu}{cf_s}$. Let

$$\mathbf{G} = [\boldsymbol{\chi}_1^{\theta} \ \cdots \ \boldsymbol{\chi}_I^{\theta}, \boldsymbol{\chi}_1^{\mathbf{v}} \ \cdots \ \boldsymbol{\chi}_I^{\mathbf{v}}], \tag{40}$$

then the CRB matrix for the parameter vector $\boldsymbol{\eta}$ is given by

$$CRB(\boldsymbol{\eta}) = [2\Re(\mathbf{G}^H\mathbf{Q}^{-1}\mathbf{G})]^{-1}. \tag{41}$$

## References

[1] V. Winkler, Range doppler detection for automotive FMCW radars, in: Proceedings of the European Microwave Conference, 2007, pp. 1445–1448, doi:10.1109/EUMC.2007.4405477.
[2] N. Jiang, R. Wu, J. Li, Super resolution feature extraction of moving targets, IEEE Trans. Aerosp. Electron. Syst. 37 (3) (2001) 781–793, doi:10.1109/7.953236.
[3] B. Xerri, J.-F. Cavassilas, B. Borloz, Passive tracking in underwater acoustic, Signal Process. 82 (8) (2002) 1067–1085.
[4] S. Liu, Z. Zeng, Y.D. Zhang, T. Fan, T. Shan, R. Tao, Automatic human fall detection in fractional fourier domain for assisted living, in: Proceedings of the IEEE International Conference on Acoustics, Speech and Signal Processing (ICASSP), IEEE, 2016, pp. 799–803.
[5] K. Yamaguchi, M. Saito, K. Miyasaka, H. Matsue, Design and performance of a 24 GHz band FM-CW radar system and its application, in: Proceedings of the IEEE Asia Pacific Conference on Wireless and Mobile, 2014, pp. 226–231, doi:10.1109/APWiMob.2014.6920270.
[6] F. Belfiori, W. van Rossum, P. Hoogeboom, Application of 2D MUSIC algorithm to range-azimuth FMCW radar data, in: Proceedings of the Ninth European Radar Conference (EuRAD), 2012, pp. 242–245.
[7] M.D. Zoltowski, K.T. Wong, Esprit-based 2-D direction finding with a sparse uniform array of electromagnetic vector sensors, IEEE Trans. Signal Process. 48 (8) (2000) 2195–2204.
[8] H. Al-Tous, I. Barhumi, N. Al-Dhahir, Atomic-norm for joint data recovery and narrow-band interference mitigation in OFDM systems, in: Proceedings of the IEEE Twenty-Seventh Annual International Symposium on Personal, Indoor, and Mobile Radio Communications (PIMRC), 2016, pp. 1–5, doi:10.1109/PIMRC.2016.7794716.
[9] L. Zheng, X. Wang, Super-resolution delay-doppler estimation for OFDM passive radar, IEEE Trans. Signal Process. 65 (9) (2017) 2197–2210, doi:10.1109/TSP.2017.2659650.
[10] J. Yu, J. Xu, Y.N. Peng, X.G. Xia, Radon-fourier transform for radar target detection (III): optimality and fast implementations, IEEE Trans. Aerosp. Electron. Syst. 48 (2) (2012) 991–1004, doi:10.1109/TAES.2012.6178044.
[11] F. Roos, D. Ellenrieder, N. Appenrodt, J. Dickmann, C. Waldschmidt, Range migration compensation for chirp-sequence based radar, in: Proceedings of the German Microwave Conference (GeMiC), 2016, pp. 317–320, doi:10.1109/GEMIC.2016.7461620.
[12] Z. Sun, X. Li, W. Yi, G. Cui, L. Kong, Detection of weak maneuvering target based on keystone transform and matched filtering process, Signal Process. 140 (2017) 127–138, doi:10.1016/j.sigpro.2017.05.013. http://www.sciencedirect.com/science/article/pii/S0165168417301846
[13] N. Jiang, J. Li, Multiple moving target feature extraction for airborne HRR radar, IEEE Trans. Aerosp. Electron. Syst. 37 (4) (2001) 1254–1266, doi:10.1109/7.976963.
[14] J. Li, G. Liu, N. Jiang, P. Stoica, Moving target feature extraction for airborne high-range resolution phased-array radar, IEEE Trans. Signal Process. 49 (2) (2001) 277–289, doi:10.1109/78.902110.
[15] W. Roberts, P. Stoica, J. Li, T. Yardibi, F.A. Sadjadi, Iterative adaptive approaches to MIMO radar imaging, IEEE J. Sel. Top. Signal Process. 4 (1) (2010) 5–20, doi:10.1109/JSTSP.2009.2038964.
[16] N. Petrov, F.L. Chevalier, Iterative adaptive approach for unambiguous wideband radar target detection, in: Proceedings of the European Radar Conference (EuRAD), 2015, pp. 45–48, doi:10.1109/EuRAD.2015.7346233.
[17] N. Petrov, F.L. Chevalier, Fast implementation of iterative adaptive approach for wideband unambiguous radar detection, in: Proceedings of the Twenty-Third European Signal Processing Conference (EUSIPCO), 2015, pp. 1207–1211, doi:10.1109/EUSIPCO.2015.7362575.
[18] T. Shan, S. Liu, Y.D. Zhang, M.G. Amin, R. Tao, Y. Feng, Efficient architecture and hardware implementation of coherent integration processor for digital video broadcast-based passive bistatic radar, IET Radar Sonar Navig. 10 (1) (2016) 97–106.
[19] J. Xu, J. Yu, Y.N. Peng, X.G. Xia, Radon-fourier transform for radar target detection (II): blind speed sidelobe suppression, IEEE Trans. Aerosp. Electron. Syst. 47 (4) (2011) 2473–2489, doi:10.1109/TAES.2011.6034645.
[20] D. Zoeke, A. Ziroff, Phase migration effects in moving target localization using switched MIMO arrays, in: Proceedings of the European Radar Conference (EuRAD), 2015, pp. 85–88, doi:10.1109/EuRAD.2015.7346243.
[21] H. Wang, M. Kaveh, Coherent signal-subspace processing for the detection and estimation of angles of arrival of multiple wide-band sources, IEEE Trans. Acoust. Speech Signal Process. 33 (4) (1985) 823–831, doi:10.1109/TASSP.1985.1164667.

[22] H. Hung, M. Kaveh, Focussing matrices for coherent signal-subspace processing, IEEE Trans. Acoust. Speech Signal Process. 36 (8) (1988) 1272–1281, doi:10.1109/29.1655.
[23] A. Belouchrani, M.G. Amin, Time-frequency MUSIC, IEEE Signal Process. Lett. 6 (5) (1999) 109–110.
[24] Y. Zhang, M.G. Amin, Blind separation of nonstationary sources based on spatial time-frequency distributions, EURASIP J. Appl. Signal Process. 2006 (2006) 198–198.
[25] A.B. Gershman, M.G. Amin, Wideband direction-of-arrival estimation of multiple chirp signals using spatial time-frequency distributions, IEEE Signal Process. Lett. 7 (6) (2000) 152–155.
[26] D. Oh, J.H. Lee, Low-complexity range-azimuth FMCW radar sensor using joint angle and delay estimation without SVD and EVD, IEEE Sens. J. 15 (9) (2015) 4799–4811, doi:10.1109/JSEN.2015.2428814.
[27] S. Kim, D. Oh, J. Lee, Joint DFT-ESPRIT estimation for TOA and DOA in vehicle FMCW radars, IEEE Antennas Wirel. Propag. Lett. 14 (2015) 1710–1713, doi:10.1109/LAWP.2015.2420579.
[28] S. Hong, X. Wan, H. Ke, Spatial difference smoothing for coherent sources location in MIMO radar, Signal Process. 109 (2015) 69–83, doi:10.1016/j.sigpro.2014.09.037. http://www.sciencedirect.com/science/article/pii/S0165168414004642.
[29] M. Haardt, F. Roemer, G. Del Galdo, Higher-order SVD-based subspace estimation to improve the parameter estimation accuracy in multidimensional harmonic retrieval problems, IEEE Trans. Signal Process. 56 (7) (2008) 3198–3213.
[30] M.A. Richards, The keystone transformation for correcting range migration in range-doppler processing, Pulse 1000 (2014) 1.
[31] Y. Saad, Iterative Methods for Sparse Linear Systems, volume 82, SIAM, 2003.
[32] B.N. Parlett, The Symmetric Eigenvalue Problem, SIAM, 1998.
[33] M. Steiner, K. Gerlach, Fast converging adaptive processor or a structured covariance matrix, IEEE Trans. Aerosp. Electron. Syst. 36 (4) (2000) 1115–1126, doi:10.1109/7.892662.
[34] P. Stoica, R.L. Moses, Spectral Analysis of Signals, Pearson/Prentice Hall Upper Saddle River, NJ, 2005.